Journal of Luminescence 190 (2017) 100–107

Contents lists available at ScienceDirect

Journal of Luminescence

journal homepage: www.elsevier.com/locate/jlumin

Effect of cobalt doping on structural, thermo and photoluminescent properties of ZnO nanopowders

N. Pushpa, M.K. Kokila*

Department of Physics, Bangalore University, Bangalore 560056, India

ARTICLE INFO

Keywords:
Solution combustion
Phosphor
Micro-Raman
ZnO
Luminescence

ABSTRACT

Nanocrystalline cobalt doped zinc oxide nanoparticles are synthesized by solution combustion method using sucrose as a fuel. The synthesized samples are characterized by XRD, SEM, FTIR, Micro-Raman, UV–Visible techniques. XRD studies confirm that both undoped and Co doped samples exhibit hexagonal wurtzite structure with crystallite size ~30 nm for undoped ZnO and 25–18 nm for Co doped ZnO samples. Both undoped and Co doped samples exhibit Raman peaks at 432, 502, 578, 681, 766, 865, 967 and 1175 cm^{-1}. Intensity of E_2 (high) mode of ZnO appeared at 432 cm^{-1} and decreases drastically with increase in cobalt concentration. Photoluminescence (PL) of all the samples shows violet emission peaks at 361, 398 nm, blue emission peaks at 468,492 nm and weak green emission peaks at 517 and 567 nm. PL intensity is found to decrease with the increase in Co^{2+} doping. Thermoluminescence (TL) glow curves of Co doped ZnO nano crystalline phosphors are γ-irradiated in the dose range 0.1–5.0 kGy. Prominent glow peaks at 412 and 575 K are observed for all the exposed doses without changing its glow peak structure. TL intensity increases linearly with γ-dose up to 4 kGy. The Kinetic parameters of TL glow are calculated by deconvolution technique. Activation energy and frequency factor are found to be 1.35 eV and 2.10×10^{11} s^{-1} respectively.

1. Introduction

ZnO is a wide band gap ($E_g = 3.37$ eV) semiconductor material with a large exciton binding energy (60 meV) at room temperature and it is extensively used as optoelectronic, catalytic, gas sensing and piezo-electric material [1–3]. Furthermore, ZnO nano crystals with wide band gap energies are prospective host materials for doping luminescence centers [4]. Nano sized ZnO is considered as an efficient luminescent material over bulk ZnO due to many facts like particle size dependent band gap, thermal and chemical stability and a low production cost. On the other hand, transition metal (TM) doped semiconductor nano particles are technologically important in the production of efficient luminescent materials [5,6] with numerous applications. The normal temperature synthesis process like sol-gel method, solution combustion method, precipitation method, etc. are found suitable to produce TM ion doped ZnO of high efficiency [7–9]. However, combustion synthesis is an important powder processing technique generally used to prepare oxide materials. It involves several advantages like fast heating, short reaction time besides producing foamy, homogeneous and high surface area nano crystalline products. It has also the advantage of doping desired amount of ions in solution medium and low processing temperature leading to uniform crystallite size [10].

Thermoluminescence (TL) is used as a powerful tool to study luminescence centers responsible for the emission in materials. Numbers of thermoluminescence dosimeters (TLD) are available commercially. However, commercial TLD's are not useful for the measurement of high dose due to the saturation of TL intensity by overlapping of ionized zones. Nanomaterials find application in high dose TL dosimetry. Hence studies are still being made to improve the TL characteristics of the nano phosphors by preparing them using different methods of doping with different impurities. TL technique has many applications in industrial, medical and agriculture field and motivated researchers to develop new materials with adequate dosimetric properties [11–13].

The objective of this work is to study the effect of cobalt doping on ZnO nanoparticles and to investigate their structural and luminescent properties by using various techniques such as powder X-ray diffraction (PXRD), Fourier transform infrared spectroscopy (FTIR), Raman, UV–Vis, photoluminescence (PL) and thermoluminescence techniques. Nanophosphors have potential applications for the measurement of high dose. Therefore in the present work, TL behavior of the ZnO nano material can be tuned by doping cobalt ions and hence there is a substantial demand for the development of ZnO nanophosphor with better TL dosimetric properties.

* Corresponding author.
E-mail address: drmkkokila@gmail.com (M.K. Kokila).

http://dx.doi.org/10.1016/j.jlumin.2017.05.032
Received 27 October 2016; Received in revised form 27 March 2017; Accepted 12 May 2017
Available online 17 May 2017

2. Experimental

The Undoped and Co^{2+}(0.1–2 mol%) doped ZnO nano phosphors are synthesized using a solution combustion technique using the stoichiometric composition of Zinc nitrate ($Zn(NO_3)_2{\cdot}6H_2O$, Sigma-Aldrich 99%) Cobalt nitrate ($Co(NO_3)_2{\cdot}6H_2O$, Sigma-Aldrich 99%)) and sucrose ($C_{12}H_{22}O_{11}$, Sigma-Aldrich 99.5%)) dissolved in a minimum quantity of double distilled water in a petridish keeping total oxidizing (O) and reducing (F) valencies of the components as unity (i.e. O/F = 1). The dish containing the above solution is introduced into a preheated muffle furnace maintained at 400 ± 10 °C. At the beginning, solution undergoes spontaneous combustion. At the point of spontaneous combustion, the solution begins burning and releases heat. Then the solution vaporizes instantly and becomes a burning solid. The entire combustion process completes producing ZnO:Co^{2+} phosphor within 10–15 min [14].

The X-ray diffraction (XRD) of undoped and Co^{2+} doped ZnO phosphors are studied by Shimadzu X-ray diffractometer (PXRD-7000) using Cu Kα radiation wavelength 1.54 (Å), step size 0.02°, 1°/min). Fourier transform infrared spectrum (FTIR) is recorded using a Perkin–Elmer spectrometer (Spectrum 1000). Raman studies are carried by ID Raman micro-785 Ocean Optics microscope at 785 nm laser excitation (Resolution 10 cm^{-1}, 40X objective: > 2 μm spot size; Laser power 100 mW). The UV–Vis absorption of the samples is recorded on SL 159 ELICO UV–Vis Spectrophotometer. Photoluminescence (PL) is recorded in Hitachi F-2700 fluorescence spectrophotometer using 150 W Xenon lamp as excitation source (Resolution: 1.5 nm). Thermoluminescence (TL) is recorded using Harshaw TLD reader (Model-3500) in the temperature range 323–550 K at an heating rate of 5 K s^{-1}. For TL measurements, 40 mg of nanophosphor are exposed to γ- rays (^{60}Co) in a dose range 0.05–10.00 kGy.

3. Results and discussions

3.1. X-ray diffraction

The X-ray diffraction patterns of undoped and Co (0.1–2 mol%) doped ZnO nano phosphors are as shown in Fig. 1(a). All the diffraction peaks are indexed to hexagonal wurtzite structure and well matched to JCPDS Card no. 36–1451. In Fig. 1(a) all the diffraction peaks are broad and it is an indication of nano sized particles. No impurity peaks are observed even after addition of 2 mol% Co ions in ZnO indicates a well crystallized ZnO material is easily obtained without calcinations. The average crystallite size is estimated using Scherer's equation $D = k\lambda/\beta\cos\theta$, where' λ' is the wavelength of X-rays (0.154 nm), 'β' is the full width at half maximum (in radians), 'θ' the diffraction angle and 'k' shape factor (0.9). The crystallite size is found to be in the range 30 nm for undoped ZnO and with the addition of Co ions in ZnO matrix. The crystallite size reduces to 18 nm after 2 mol% Co doping (Table 1). It is observed that, the crystallite size decreases with increase in Co ion concentration. The lattice undergoes distortion as revealed by the ionic radii of Zn^{2+}(0.060 nm) and Co^{2+}(0.058 nm), the crystallite size decreases and diffraction peak (100) have been shifted to lower 2θ angle as shown in Fig. 1(b) [15].

Structural parameters such as lattice parameters and unit cell volumes for hexagonal ZnO nano particles are calculated from the lattice geometry equations [16].

$$\frac{1}{d^2} = \frac{4}{3}\left[\frac{h^2 + hk + k^2}{a^2}\right] + \frac{l^2}{a^2} \quad (1)$$

$$V = \frac{\sqrt{3}\,a^2c}{2} = 0.866a^2c \quad (2)$$

where a and c are the lattice parameters and h, k, and l are the Miller indices and d_{hkl} is the inter planer spacing, which can be calculated from Bragg's law

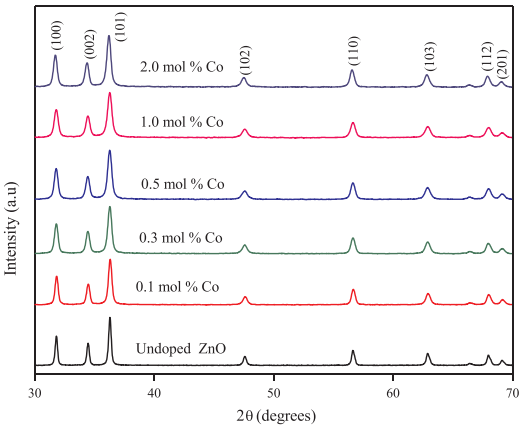

(a) X-ray diffraction patterns of undoped and Co (0.1–2 mol %) doped ZnO

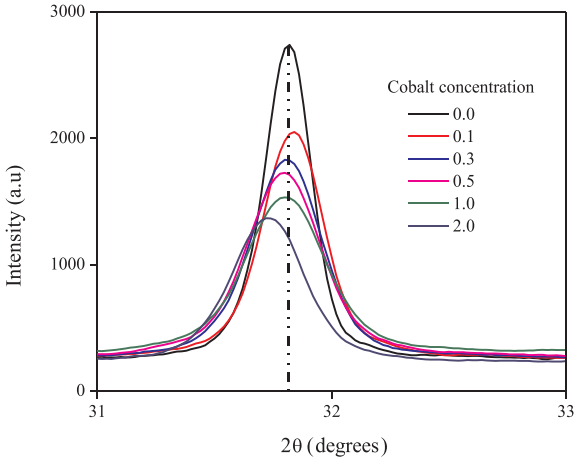

(b) Shifting of XRD (100) peak with Co doping

Fig. 1. (a) X-ray diffraction patterns of undoped and Co (0.1–2 mol%) doped ZnO. (b) Shifting of XRD (100) peak with Co doping.

Table 1
Structural parameters of undoped and cobalt doped ZnO.

Cobalt concentration (mol %)	Crystallite size (nm)	Lattice parameters (Å)		Volume of unit cell $(Å)^3$
		a	c	
0.0	30.00 ∓0.5	3.324	5.191	49.669
0.1	26.41 ∓0.8	3.331	5.230	50.253
0.3	25.00 ∓0.1	3.333	5.234	50.352
0.5	24.80 ∓0.3	3.339	5.239	50.582
1.0	19.23 ∓0.7	3.345	5.246	50.832
2.0	18.00 ∓0.2	3.355	5.258	51.253

$$2d\sin\theta = n\lambda \quad (3)$$

The changes in a and c parameters are observed due to the incorporation of Co dopant, as shown in Table 1. The volume of the unit cell increases with the increase in the Co doping level, which is shown in Fig. 2(a). According to Vegard's law, higher doping levels could increase the volume of the unit cell. The incorporation of Co^{2+} ions into the ZnO lattice could be easily identified from the fact that variation of lattice constants values with cobalt doping as shown in Fig. 2(b).

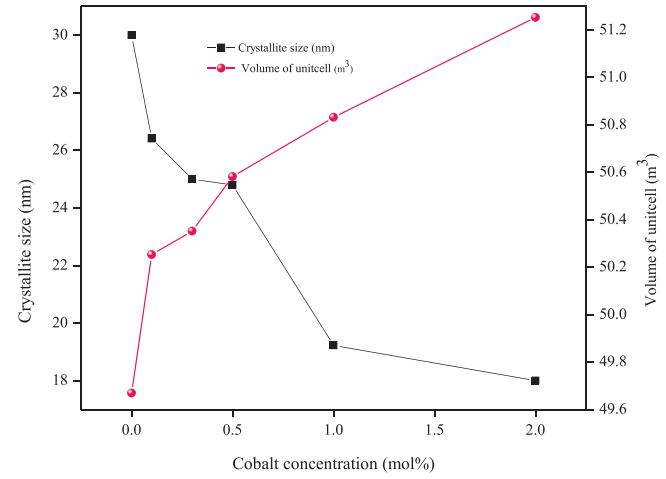

(a) Variation of crystallite size and unitcell volume with cobalt concentration

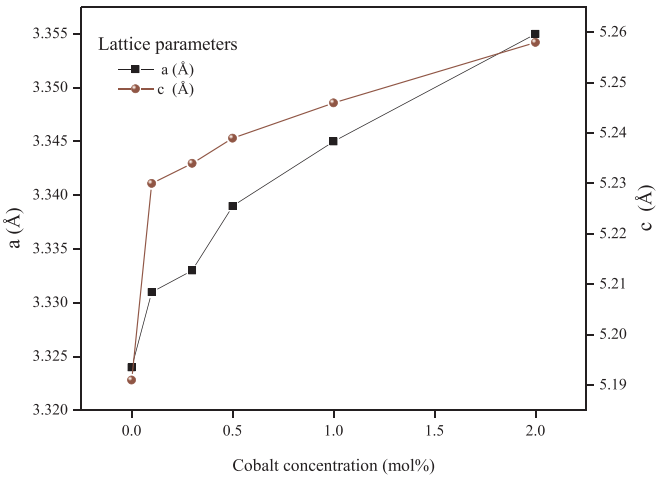

(b) Variation of lattice parameters with cobalt concentration

Fig. 2. (a) Variation of crystallite size and unitcell volume with cobalt concentration. (b) Variation of lattice parameters with cobalt concentration.

3.2. Scanning electron microscopy

The scanning electron micrograph of undoped and 1 mol% Co doped ZnO is shown in Fig. 3. The micrograph shows particles are agglomerated with large grain structure, fluffy, and porous in nature. The agglomeration of ZnO nanoparticles is due to minimizing in their surface free energy. Presence of voids and porous morphology in these samples is due to the release of gases during the combustion process [14]. It is observed that the Co doped ZnO samples are more agglomerated than the undoped samples.

3.3. FTIR and Micro-Raman studies

The FTIR measurements of undoped and Co doped samples are performed in the wavenumber range $400-4000\ cm^{-1}$ using a KBr pellet technique at room temperature as shown in Fig. 4. The broad transmission peak at $3430\ cm^{-1}$ represents the stretching vibration of the O–H group. The bending vibration of the interlayer water molecule appeared with the typical band at $1635\ cm^{-1}$. The peaks appeared between 1300 and $1600\ cm^{-1}$ are attributed to C=O stretching modes [15]. The band at $458\ cm^{-1}$ is assigned to the stretching mode of ZnO. The shift in the peak position of the ZnO bands reflects the Zn–O–Zn network perturbed by the presence of Co in its environment [17]. This shift in the Zn–O stretching peak position with cobalt doping is shown in Fig. 4.

In order to investigate the influence of cobalt doping on the Raman scattering in ZnO nanostructures, room temperature micro Raman spectra of all samples are explored. ZnO is one of the simplest uniaxial crystal with wurtzite structure belongs to the *P*63*mc* space group. It is well known that wurtzite ZnO has eight sets of characteristic optical phonon modes at the center of brillouin zone Γ point. Group theory predicts of the following optical modes.

$$\Gamma_{Opt} = 1A_1 + 2B_1 + 1E_1 + 2E_2$$

Where E modes are twofold degenerate. The B_1 modes are silent, i.e. IR and Raman inactive, and A_1, E_1 and E_2 modes are Raman active. In addition, A_1 and E_1 are infrared active, and split into longitudinal and transverse optical component (LO and TO). The mode assignment at ambient conditions is well established in the literature [18]. It is known that the E_2 (low) mode in zinc oxide is associated with the vibration of the heavy Zn sub-lattice and the E_2 (high) mode involves only the oxygen atoms. The micro-Raman spectra of undoped and Co doped ZnO nanoparticles are shown in Fig. 5. It is observed that, all the samples exhibit Raman peaks at 432, 502, 578, 681, 766, 865, 967 and $1175\ cm^{-1}$. The intensity of E2 (high) mode of ZnO appeared at about $432\ cm^{-1}$ decreased drastically on increasing the cobalt concentration in the samples. The slight shift in the peak position after cobalt doing is observed is shown in the inset of the Fig. 5. We can say that the incorporation of cobalt into ZnO nanoparticles reduces their crystallinity and the drastic reduction in intensity might be due to the breakdown of translational crystal symmetry by the incorporated defects, reduction in crystallite size [19]. The A_1 (LO) and A_2 (LO) phonon modes of ZnO nanoparticles are observed at 578 and $1175\ cm^{-1}$, respectively. The peaks at 502, 681, 766, 865 and $967\ cm^{-1}$ are due to multi phonon modes [19–21]. The detailed assignments of each mode for all the peaks are tabulated in the Table 2.

3.4. UV–Visible spectroscopy

The UV–Visible absorption spectra of undoped and Co doped ZnO nanophosphors of samples shows strong absorption maximum at 375 nm (Fig. 6). Bandgap (E_g) has been calculated using Tauc plot [22]. Fig. 7 shows the plots of $(\alpha h\nu)^2$ versus $h\nu$ for undoped and Co doped ZnO samples. The values of E_g have been estimated at the intersection of the tangents drawn on the curves. The E_g is found to be 3.12 eV for undoped ZnO sample and increases to 3.41 eV for 2 mol% Co concentration in the sample. This change in the value of E_g depends on several factors such as grain size, carrier concentration, lattice strain, etc. Variation of the band gap and crystallite size of samples with respect to cobalt concentration is shown in Fig. 8. Generally, excess carriers through doping donated by impurities lead to the blue shift of optical band-to-band transitions of the Co doped ZnO nano particles. The blue shift of absorption peak and the broadening of the absorption onset increase in Co dopant concentration, indicating that more impurity levels occurred within the band gap, and hence the band gap increased [23].

3.5. Photoluminescence

PL emission spectra of undoped and Co^{2+} doped ZnO recorded in the range 350–800 nm are shown in Fig. 9. PL emission shows sharp UV and broad visible bands. PL emission spectra of cobalt undoped ZnO shows are similar emission of undoped, but shows variation in PL intensity with cobalt concentration in addition to the formation of defects. It is observed that all the samples emission with peaks at 361, 398 nm in the violet region, The UV peaks usually considered as the characteristic emission of ZnO and are attributed to the near band edge

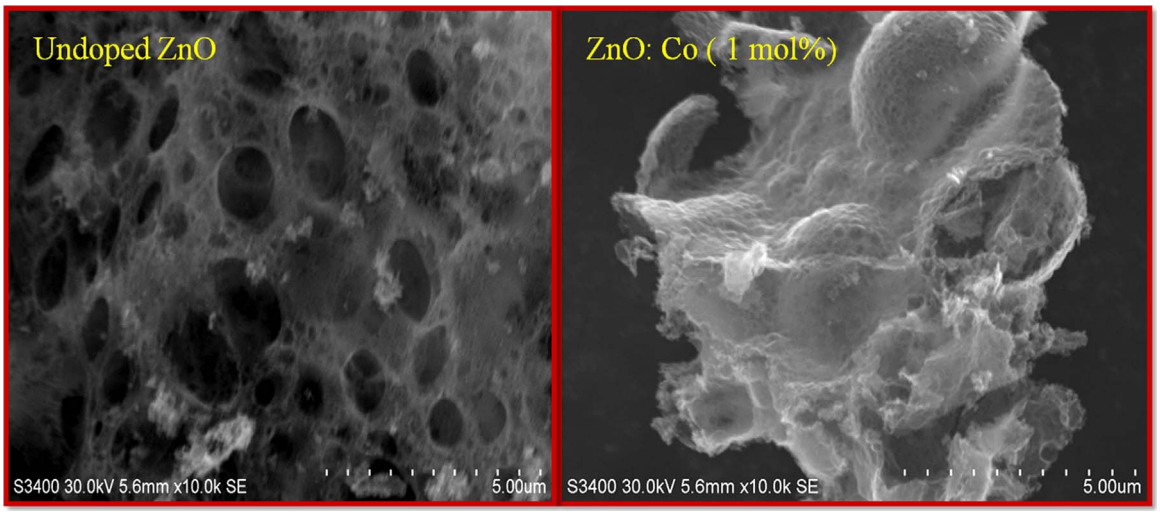

Fig. 3. Scanning electron micrographs (SEM) of undoped and 1 mol% Co doped ZnO.

(NBE) exciton emission, which originates from free exciton [19,21]. Broad visible band is observed due to formation of native defects across the band gap of ZnO. UV and Visible bands in undoped and Co doped ZnO have multiple emissions and frequently assigned to different defects. Blue emission peaks at 468,492 nm and weak green emission peaks at 517, and 567 nm. The broad blue band emission peaks are assigned to surface defects such as oxygen vacancies (V_o) and Zinc interstitials (Zn_i). The green emission origin is generally assigned to the radiative recombination of photo generated holes in the valence band with electrons in singly occupied oxygen vacancies [20,22]. The PL emission intensity is found to decrease with the increase in cobalt concentration as shown in the inset of Fig. 9. UV emission peak (398 nm) is becoming very broad with an increase in cobalt concentration and peak shifts towards lower energy due to carrier-impurity and carrier-phonon interactions leading to broadening of the band gap. After cobalt doping, creation of holes in the valence band leads to shift in Fermi level to a lower position, thus widening (blue shift) the band gap. This blue shift is responsible for the NBE emission of higher energy due to the formation of Co interstitial defects. Further from our

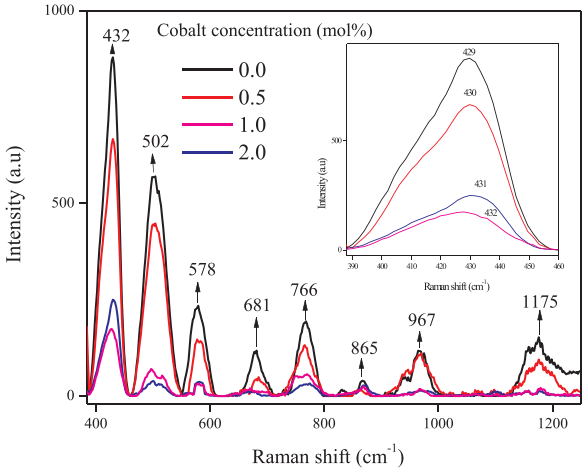

Fig. 5. Micro-Raman studies of undoped and Co doped ZnO nano particles.

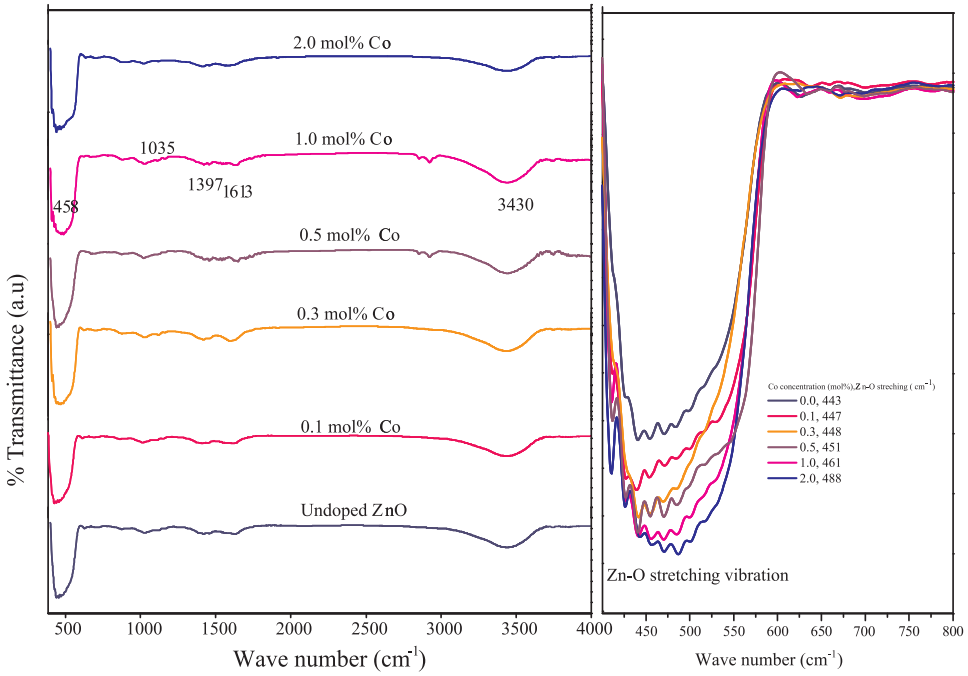

Fig. 4. FTIR studies of undoped and Co doped ZnO nanophosphors.

Table 2
Assignment of Raman modes of undoped and cobalt doped ZnO nanoparticles.

Cobalt concentration (mol %)	Wavenumber (cm^{-1})			
	E2 (high)	A_1 (LO)	A_2 (LO)	Multi phonon modes
0.0	429	578	1175	502, 680,767, 866, 966
0.5	430	579	1176	500, 682, 768, 870, 969
1.0	432	580	1178	497, 683, 770, 773, 967
2.0	431	581	1179	497, 687, 773, 775, 970

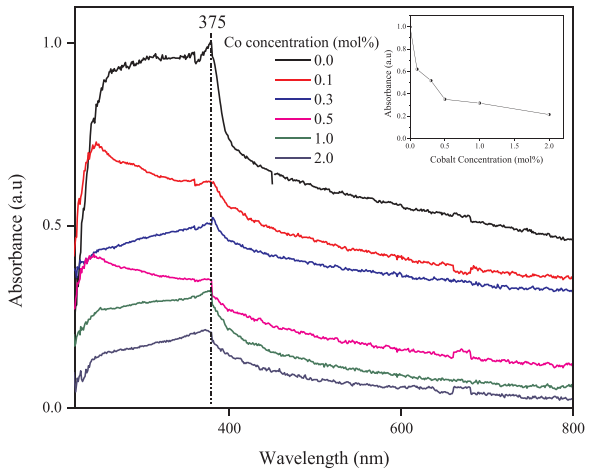

Fig. 6. UV–Visible absorption studies of undoped and Co doped ZnO nanophosphor.

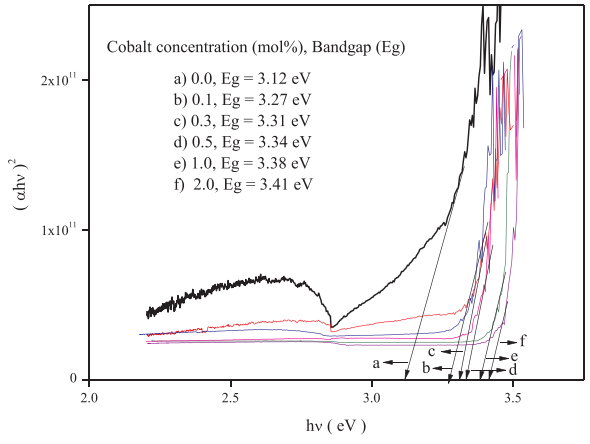

Fig. 7. $(\alpha h\nu)^2$ versus hν for undoped and Co doped ZnO samples.

previous reports on PL studies of ZnO:Mg^{2+} nanoparticles prepared from urea fuel show PL emission peaks at same position as compared with undoped and Co doped ZnO nanoparticles, but PL intensity enhanced after Mg^{2+} doping [24]. With the cobalt doping quenching of PL emission is observed.

3.6. Thermoluminescence

TL glow curves of ZnO nanopowders irradiated with gamma (γ) rays for a dose range of 0.05–10 kGy is shown in Fig. 10. TL glow curves are recorded at a heating rate of 5 K s^{-1} and well resolved broad glow peaks at 500 K and 675 K are observed for all the doses. The broad shape of the TL glow peak suggests the distribution of number traps in the band gap of ZnO nanostructures. Fig. 11 shows the variation of glow

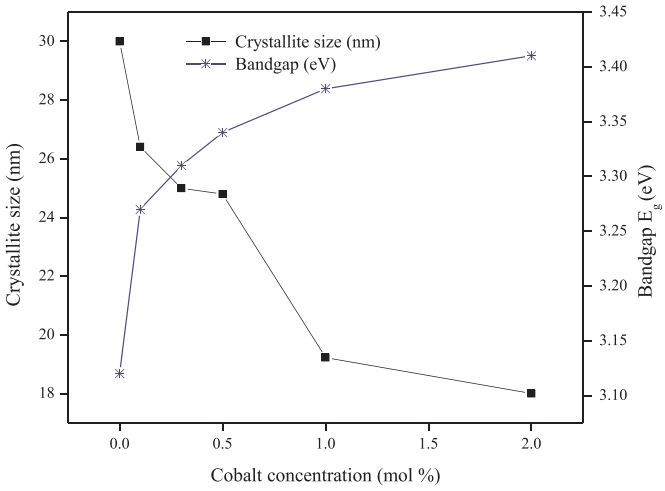

Fig. 8. Variation of bandgap and crystallite size with cobalt concentration.

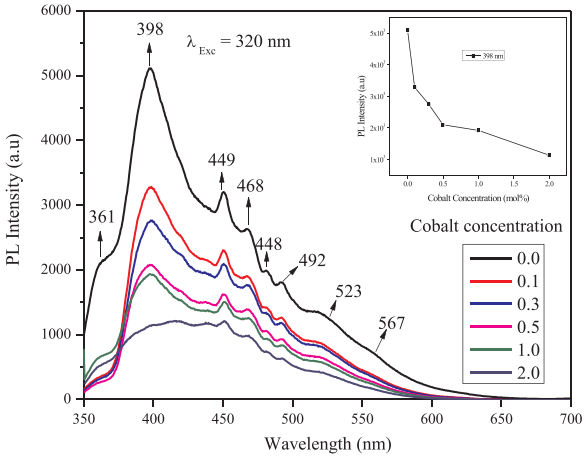

Fig. 9. PL emission of undoped and Co doped ZnO nanoparticles.

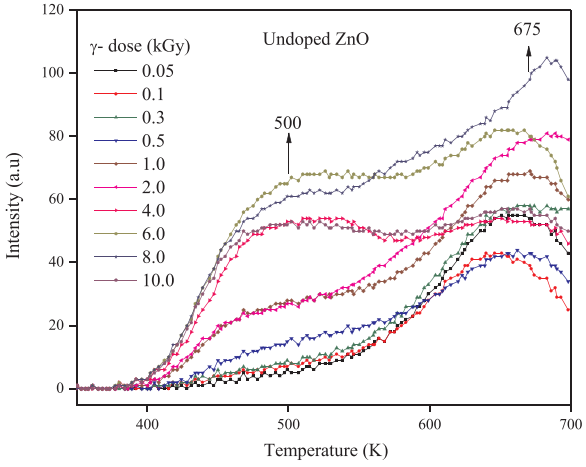

Fig. 10. TL glow curves of ZnO nano powders irradiated with gamma (γ) rays.

peak intensity with γ-dose. It is observed that low temperature glow peak intensity shows linear response with increase of gamma dose upto 1 kGy, sub linear up to 6 kGy and then decreases with further increase of γ-dose and the glow peak position is unaltered with γ-doses. The increase in intensity of TL glow peak with irradiation dose makes clear indication that more oxygen vacancies helps in the creation of traps in the band gap of the material up to 6 kGy [25]. The decrease in TL intensity after the 6 kGy may be due to formation of cluster of oxygen

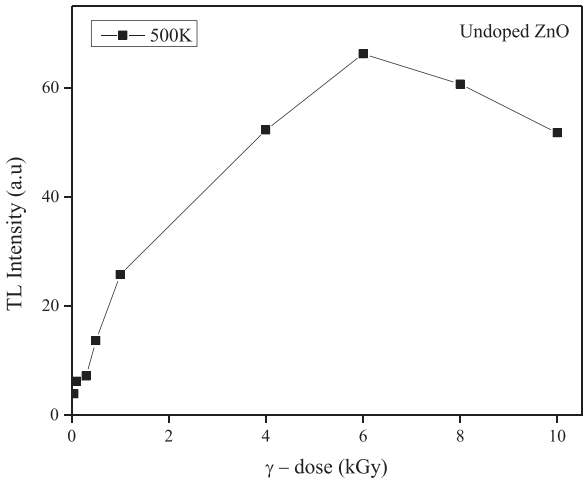

Fig. 11. Variation of glow peak intensity with γ-irradiation dose for undoped ZnO.

vacancies leading to complex defects. High temperature TL glow peak not exhibit linear response with γ-dose.

TL glow curves of cobalt doped ZnO samples irradiated with gamma rays for a dose of 2 kGy are shown in Fig. 12. Cobalt doped samples shows high temperature TL glow peak ~575 K upto 0.3 mol% doping and for higher concentration of cobalt the samples exhibit well structured TL glow curve with peaks at ~411 K along with high temperature TL glow peak. This is due to the cobalt doping in the material could help in generating more number of electron/hole traps and luminescent centers responsible for TL. Variation of TL glow peak intensity with Co^{2+} concentration is shown in Fig. 13. Maximum TL intensity is observed for the concentration of 1 mol%. This could be due to the increase in the number of luminescent centers and also due to the increase in the probability of energy transfer from the traps to the luminescent centers and then decreases with the further increase of the Co^{2+} concentration. However, it is concentration quenching [26]. Hence this concentration (1 mol%) is exposed to gamma rays for various doses to study its TL response. Fig. 14 shows the TL glow curves of Co^{2+} (1 mol%) doped ZnO nanophosphor γ-irradiated in the dose range 0.05-6.0 kGy at an heating rate of 5 K s^{-1}. The resulting glow peaks at 411 and 577 K are prominent and are observed for all the exposed doses without alter its glow peak structure. Variation of TL glow peak intensity for different γ-doses are plotted and shown in Fig. 15. TL intensity increases linearly with γ-dose upto 4 kGy. This behavior of the sample is useful for dosimetric application. The increase in TL intensity suggests that more number of electron and hole traps are

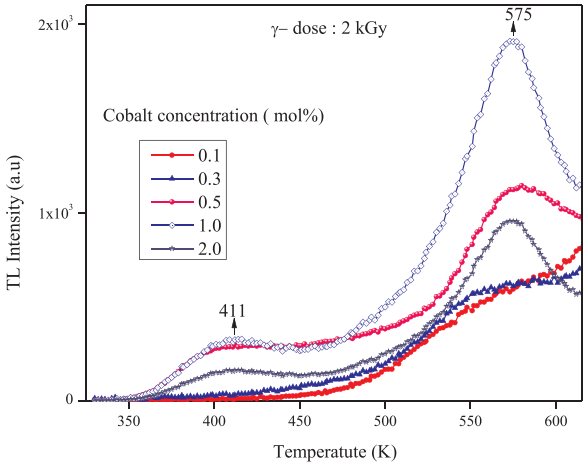

Fig. 12. TL glow curves of cobalt doped ZnO samples irradiated with gamma ray dose of 2 kGy.

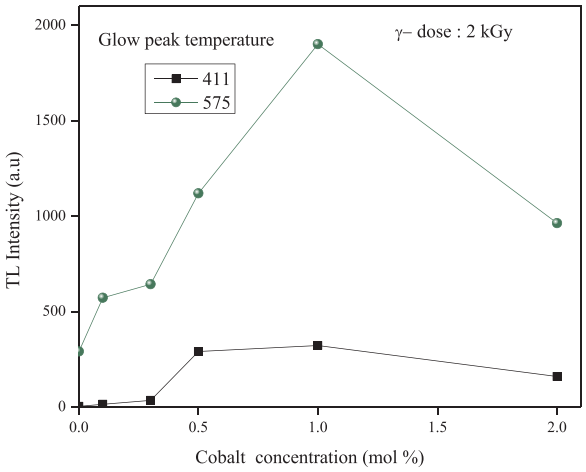

Fig. 13. Variation of glow peak intensity with cobalt concentration.

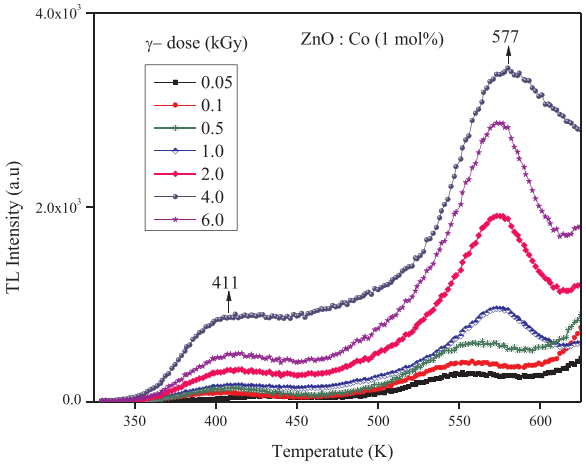

Fig. 14. TL glow curves of Co doped ZnO nano crystalline phosphor.

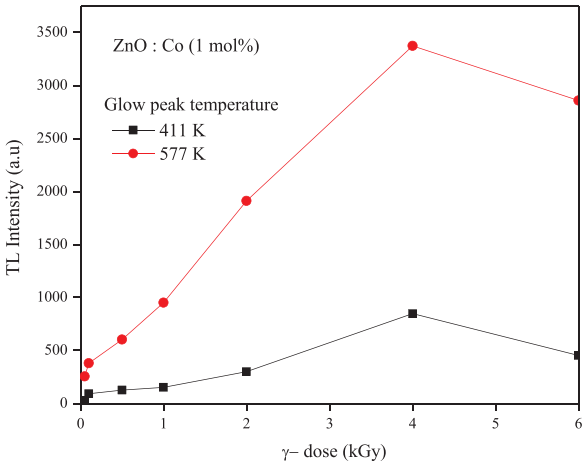

Fig. 15. Variation of glow peak intensity with γ- irradiation dose for Co doped ZnO nanophosrhors.

created by irradiation and supply thermal energy, these traps escapes from the trapped centers and recombine with contradictory centers at the luminescent center (LC) which leads to TL signal with the increase of γ-dose. After the dose of 4.0 kGy, the TL intensity decreases with further increase of γ-dose due to formation of complex defects as a result reduction of recombination centers [27]. As a result of more number of lattice defects/ trap formation and found to be smaller for the samples irradiated with lower γ-dose due to creation of lesser

defects/traps. The linear behavior of TL intensity is explained based on defect interaction model. According to this model, recombination within the trapping center/luminescent center (TC/LC) complex dominates at low dose levels and leads to a linear response, whereas charge carrier migration leads to inter-complex recombination, i.e. increase in the luminescence efficiency at higher dose levels [28]. The presence two kinds of glow peaks at 411 K and 577 K indicate that two kinds of trapping centers (shallow/deep) are created due to γ-irradiation [29,30]. Further, the TL results of the present work are compared with previously reported TL properties of gamma irradiated on Mg^{2+} doped ZnO [24]. ZnO:Mg^{2+} exhibits glow peak at 618 K with a weak shoulder at 474 K. ZnO:Co^{2+} exhibit a well resolved prominent TL glow peaks at 411 and 575 K. The high temperature peak (575 K) shows relatively high intensity, good stability and responds to γ-doses. Further, ZnO:-Co^{2+} shows the TL intensity increases linearly up to 4 kGy where as ZnO:Mg^{2+} shows the linearity up to 1 kGy. However, a detailed investigation needs to be carried out on ZnO:Co^{2+} for its suitability in high dose radiation dosimetry.

3.7. Calculation of kinetic parameters

The detailed studies of TL kinetic parameters qualitatively describe the trapping or emitting centers responsible for TL process. Kinetic parameters provide valuable information for the TL mechanism responsible for dosimetric applications. TL glow curves are deconvoluted using a computerized glow curve deconvolution method (GCD) [31] using equation for general order of kinetics suggested by Kitis et al. [32].

The equation for general order kinetics which is used for glow curve deconvolution as follows,

$$I(t) = I_m b^{\frac{b}{b-1}} \left(\frac{E}{kT}\frac{T-T_m}{T_m}\right) \left[(b-1)(1-\Delta)\frac{T^2}{T_m^2}\exp\left(\frac{E}{kT}\frac{T-T_m}{T_m}+Z_m\right)\right]^{-\frac{b}{b-1}} \quad (4)$$

with $\Delta = 2kT/E$, $\Delta_m = 2kT_m/E$, $Z_m = 1 + (b\text{-}1)\,\Delta_m$.

where 'k' is Boltzmann constant (8.6×10^{-5} eV K^{-1}), I_m is the intensity of glow peak, β the linear heating rate and b represents the order of kinetics and T_m refers to glow peak temperature. For glow curve fitting software package in Microsoft Excel has been used [31]. In order to fit the glow peak, we have to input the arbitrary values for the parameters I_m, T_m, E and b for each glow peak. After the curve fitting we will get the net values of I_m, T_m, E and b. The frequency factor and Figure of merit (FOM) values are determined using expressions given below

$$\frac{\beta E}{kT_m^2} = s\exp\frac{-E}{KT_m}[1+(b-1)\Delta_m] \quad (5)$$

$$FOM = \frac{\sum|TL_{exp}-TL_{the}|}{\sum TL_{the}} \quad (6)$$

Here TL_{exp} and TL_{the} represent TL intensity of experimental and theoretical glow curves respectively. The goodness of fit is decided by FOM. The values are considered when the FOM value less than 5%. In the present work the FOM is 2% and 1.8% for undoped Co^{2+} doped ZnO, it indicating that experimentally deconvoluted glow curve well correlated with theoretical fitted curve. Figs. 16 and 17 shows deconvoluted TL glow curves of undoped and Co^{2+}(1 mol%) doped ZnO irradiated to γ- dose of 6 kGy and 2 kGy respectively. The undoped ZnO TL glow curve deconvoluted into five peaks at 461, 507, 556, 610, 672 K and cobalt doped ZnO nanophosphors are deconvoluted in to five TL peaks at 400, 436, 482, 528 and 575 K are due to distribution of traps in the forbidden region. The calculated kinetic parameters are given in Table 3. It is found that the low and high temperature TL

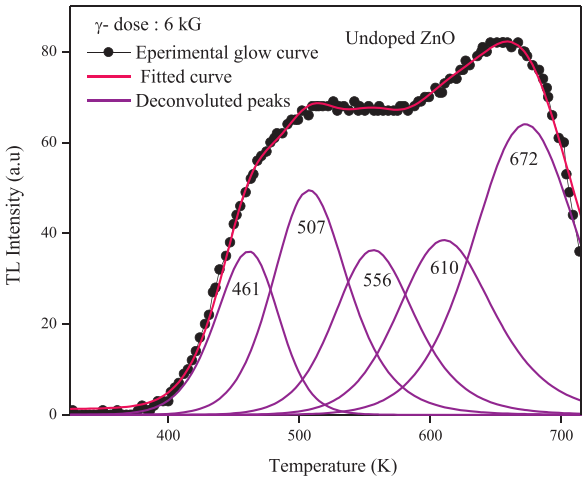

Fig. 16. Deconvoluted TL glow curves of undoped ZnO irradiated at γ- dose of 6 kGy.

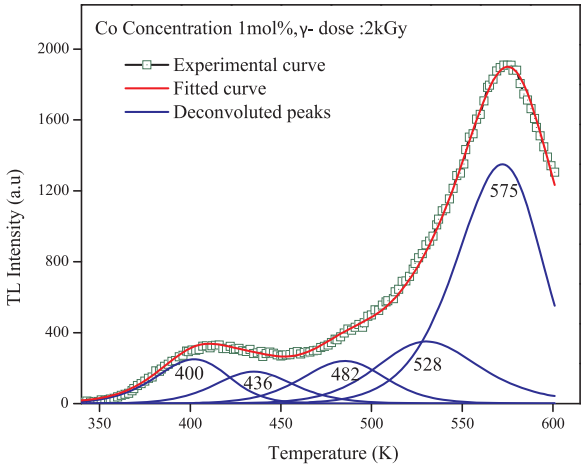

Fig. 17. Deconvoluted TL glow curves of Co doped ZnO Nanophoshor.

Table 3
Kinetic parameters of undoped and Co doped ZnO nanophosphors.

Sample	T_m (K)	b	E_{av} (eV)	s (s^{-1})	FOM (%)
Undoped ZnO (γ - dose 6 kGy)	461	1.0	0.95	1.63×10^{9}	
	507	2.0	1.08	1.22×10^{10}	
	556	2.0	1.20	1.57×10^{10}	2.0
	610	2.0	1.22	2.10×10^{9}	
	672	1.8	1.25	3.54×10^{8}	
Co doped ZnO (γ - dose 2 kGy)	400	1.4	0.80	3.56×10^{9}	
	436	1.8	1.00	1.33×10^{11}	
	482	1.6	1.10	8.39×10^{10}	1.8
	530	2	1.20	7.12×10^{10}	
	575	2	1.35	2.10×10^{11}	

glows, obeys the first and second order kinetics, respectively. It indicates the low temperature glow, the trapped electron direct recombine with hole center while high temperature glows exhibits retrapping and then recombine with contradictory center at LC resulting TL signal. The activation energy of deconvoluted peaks increases with increase in glow peak temperature. This indicates that each glow peak has different trap levels in the band gap of a material and at lower temperature peaks are due to electrons being trapped at a shallow level while higher temperature peaks are due to electrons activated from deep traps. The deep level traps exhibits longer life time and low fading at room temperature, therefore the deep level traps are very important for the developing dosimeter. The obtained activation energy and frequency factor values are very close to normal lattice vibration,

therefore this material is suitable for high dose dosimetry application.

4. Conclusions

Solution combustion synthesized undoped and cobalt doped ZnO nanoparticles exhibits hexagonal wurtzite structure. Crystallite size decreased from 30 nm to 18 nm with Co doping. SEM micrographs confirm that particles are agglomerated after Co doping. Energy band gap increases with increase in Cobalt concentration and found to be 3.12 eV for pure ZnO sample and increases to 3.41 eV for 2 mol% Co^{2+}. Intensity of PL emission decreases and UV emission peak (398 nm) shows broadening with increase in cobalt concentration. TL curves of undoped nanoparticles shows low intense TL glow peaks at 500 K and 675 K and Cobalt doped nanoparticles shows high intense TL glow peaks at a ~411 K and ~575 K. TL intensity increases linearly with increase in γ- dose from 0.05 to 4 kGy. Hence, this material may be useful for high dose TL dosimetry applications in the dose range 0.05–4 kGy.

Novelty of the work

Cobalt doped Zinc oxide (ZnO:Co) nanoparticles have been prepared by a solution combustion route. The nanopowders are well characterized using different spectroscopy techniques. PL emission intensity decreases and UV emission peak (398 nm) shows broadening with increase in cobalt concentration. Thermoluminescence (TL) studies of ZnO:Co nano powders with γ- irradiation are scarce as evident from the literature. In the present studies TL intensity increases linearly with increase in γ- dose. ZnO:Co material may be useful for TL dosimetry applications in the dose range 0.05–4 kGy.

Acknowledgements

The Authors acknowledges Department of Atomic Energy and Board of Research in Nuclear Science (DAE–BRNS), BARC, India for providing financial support to carry out this research work (project No. 2011/37P/18/BRNS) and DST-PURSE project, Department of Physics, Bangalore University, Bangalore for providing facilities for Raman studies.

References

[1] Y. Ni, X. Cao, G. Wu, G. Hu, Z. Yang, X. Wei, Nanotechnology 18 (2007) 3–8, http://dx.doi.org/10.1088/0957-4484/18/15/155603.
[2] A. Janotti, C.G. Van De Walle, Phys. Rev. B – Condens. Matter Mater. Phys. 76 (2007) 1–22, http://dx.doi.org/10.1103/PhysRevB.76.165202.
[3] U. Ozgur, Y.I. Alivov, C. Liu, a. Teke, M. a. Reshchikov, S. Dogan, J. Appl. Phys. 98 (2005) 1–103, http://dx.doi.org/10.1063/1.1992666.
[4] U. Pal, R. Meléndrez, V. Chernov, Appl. Phys. Lett. 183118 (2006), http://dx.doi.org/10.1063/1.2374866.
[5] S. Kumar, K. Asokan, R.K. Singh, S. Chatterjee, D. Kanjilal, A.K. Ghosh, J. Appl. Phys. 164321 (2016), http://dx.doi.org/10.1063/1.4826525.
[6] B. Wang, C. Xia, J. Iqbal, N. Tang, Z. Sun, Y. Lv, et al., Solid State Sci. 11 (2009) 1419–1422, http://dx.doi.org/10.1016/j.solidstatesciences.2009.04.024.
[7] N. Pushpa, M.K. Kokila, N.J. Shivaramu, Nucl. Instrum. Methods Phys. Res. Sect. B Beam Interact. Mater. At. 379 (2016) 69–72, http://dx.doi.org/10.1016/j.nimb.2016.04.033.
[8] S. Rasouli, S. Jebeli, J. Alloy. Compd. 509 (2011) 1915–1919, http://dx.doi.org/10.1016/j.jallcom.2010.10.087.
[9] O.D. Jayakumar, H.G. Salunke, R.M. Kadam, M. Mohapatra, G. Yaswant, S.K. Kulshreshtha, Nanotechnology 17 (2006) 1278–1285, http://dx.doi.org/10.1088/0957-4484/17/5/020.
[10] S.T. Aruna, A.S. Mukasyan, Curr. Opin. Solid State Mater. Sci. 12 (2008) 44–50, http://dx.doi.org/10.1016/j.cossms.2008.12.002.
[11] S.P. Lochab, D. Kanjilal, N. Salah, S.S. Habib, J. Lochab, R. Ranjan, et al., J. Appl. Phys. 104 (2008) 33520, http://dx.doi.org/10.1063/1.2955459.
[12] M.S. Kulkarni, D.R. Mishra, K.P. Muthe, A. Singh, M. Roy, S.K. Gupta, et al., Radiat. Meas. 39 (2005) 277–282, http://dx.doi.org/10.1016/j.radmeas.2004.03.005.
[13] Y. Wang, B. Yang, N. Can, P.D. Townsend, J. Appl. Phys. 53508 (2011) 19–23, http://dx.doi.org/10.1063/1.3556743.
[14] K.C. Patil, M.S. Hegde, T. Rattan, S.T. Aruna, Chemistry of Nanocrystalline Oxide Materials, Combustion Synthesis, Properties and Applications, World Scientific Publishing Co. Pte. Ltd, Singapore, 2008.
[15] F. Ahmed, S. Kumar, N. Arshi, M.S. Anwar, B.H. Koo, C.G. Lee, Microelectron. Eng. 89 (2012) 129–132, http://dx.doi.org/10.1016/j.mee.2011.03.149.
[16] A. Khorsand Zak, W.H. Abd. Majid, M.E. Abrishami, R. Yousefi, Solid State Sci. 13 (2011) 251–256, http://dx.doi.org/10.1016/j.solidstatesciences.2010.11.024.
[17] P.K. Sharma, A.C. Pandey, G. Zolnierkiewicz, N. Guskos, C. Rudowicz, J. Appl. Phys. 94314 (2016) 1–6, http://dx.doi.org/10.1063/1.3256000.
[18] P.K. Giri, S. Bhattacharyya, D.K. Singh, R. Kesavamoorthy, B.K. Panigrahi, K.G.M. Nair, J. Appl. Phys. 93515 (2016), http://dx.doi.org/10.1063/1.2804012.
[19] G. Xiong, U. Pal, J.G. Serrano, J. Appl. Phys. 24317 (2016), http://dx.doi.org/10.1063/1.2424538.
[20] A.J. Cheng, Y. Tzeng, H. Xu, S. Alur, Y. Wang, M. Park, et al., J. Appl. Phys. 105 (2009), http://dx.doi.org/10.1063/1.3093877.
[21] L. Tong, T. Cheng, H. Han, J. Hu, X. He, Y. Tong, et al., J. Appl. Phys. 23906 (2016).
[22] M.K. Kavitha, K.B. Jinesh, R. Philip, P. Gopinath, H. John, Phys. Chem. Chem. Phys. 16 (2014) 25093–25100, http://dx.doi.org/10.1039/C4CP03847.
[23] R.G. Singh, F. Singh, I. Sulania, D. Kanjilal, K. Sehrawat, V. Agarwal, et al., J. Nucl. Instrum. Methods Phys. Res. Sect. B Beam Interact. Mater. At. 267 (2009) 2399–2402, http://dx.doi.org/10.1016/j.nimb.2009.04.005.
[24] N. Pushpa, M.K. Kokila, K.R. Nagabhushana, Nucl. Instrum. Methods Phys. Res. Sect. B Beam Interact. Mater. At. 379 (2016) 62–68, http://dx.doi.org/10.1016/j.nimb.2016.04.042.
[25] N.J. Shivaramu, B.N. Lakshminarasappa, K.R. Nagabhushana, F. Singh, Spectrochim. Acta – Part A Mol. Biomol. Spectrosc. 154 (2016) 220–231, http://dx.doi.org/10.1016/j.saa.2015.09.019.
[26] Puja Chawla Geeta Sharm, S.P. Lochab, Nafa singh, Chalcogenide Lett. 6 (2009) 445–453.
[27] N. Salah, S.S. Habib, Z.H. Khan, S. Al-hamedi, S.P. Lochab, J. Lumin. 129 (2009) 192–196, http://dx.doi.org/10.1016/j.jlumin.2008.09.012.
[28] S. Mahajna, Y.S. Horowitz, J. Phys. D. Appl. Phys. 30 (1999) 2603–2619, http://dx.doi.org/10.1088/0022-3727/30/18/016.
[29] P.P. Pal, J. Manam, Radiat. Phys. Chem. 88 (2013) 7–13, http://dx.doi.org/10.1016/j.radphyschem.2013.03.023.
[30] N.J. Shivaramu, B.N. Lakshminarasappa, K.R. Nagabhushana, Fouran Singh, J. Alloy. Compd. 637 (2015) 564–573.
[31] D. Afouxenidis, G.S. Polymeris, N.C. Tsirliganis, G. Kitis, Radiat. Prot. Dosim. 149 (2012) 363–370, http://dx.doi.org/10.1093/rpd/ncr315.
[32] G. Kitis, J.M. Gomez-Ros, J.W.N. Tuyn, J. Phys. D. Appl. Phys. 31 (1998) 2636–2641, http://dx.doi.org/10.1088/0022-3727/31/19/037.